Materials Chemistry and Physics 358 (2026) 132500

Contents lists available at ScienceDirect

Materials Chemistry and Physics

journal homepage: www.elsevier.com/locate/matchemphys

Catalytic performance of modified metal ion-BEA zeolite for enhanced Fenton-type reaction: Part I

V. Ivasiv [a], A.R. Bertão [a], A. Martins [b,c], N. Nunes [b,c], A.P. Carvalho [c,d], A.M. Fonseca [a,e], E. Rombi [f], J.N. Moreira [g,h], F. Baltazar [i,j], I.C. Neves [a,e,*]

[a] Chemistry Centre of the University of Minho (CQ-UM), Department of Chemistry, University of Minho, Campus de Gualtar, 4710-057, Braga, Portugal
[b] DEQ, Instituto Superior de Engenharia de Lisboa, R. Conselheiro Emídio Navarro, 1, Lisboa, Portugal
[c] Centro de Química Estrutural (CQE), Faculdade de Ciências, Institute of Molecular Sciences, Universidade de Lisboa, Lisboa, Portugal
[d] Departamento de Química e Bioquímica, Faculdade de Ciências Universidade de Lisboa, Ed.8, Campo Grande, Lisboa, Portugal
[e] CEB - Centre of Biological Engineering, University of Minho, Braga, Portugal
[f] Dipartimento di Scienze Chimiche e Geologiche, University of Cagliari, Complesso Universitario di Monserrato, Monserrato, 09042, Italy
[g] CNC-UC - Center for Neurosciences and Cell Biology, Center for Innovative Biomedicine and Biotechnology (CIBB), University of Coimbra, Rua Larga - Faculdade de Medicina, 1°andar - POLO I, 3004-504, Coimbra, Portugal
[h] Univ Coimbra - University of Coimbra, CIBB, Faculty of Pharmacy, Polo das Ciências da Saúde, Azinhaga de Santa Comba, 3000-548, Coimbra, Portugal
[i] Life and Health Sciences Research Institute (ICVS), School of Medicine, University of Minho, Campus de Gualtar, Braga, Portugal
[j] ICVS/3B's - PT Government Associate Laboratory, Braga, Guimarães, Portugal

HIGHLIGHTS

- BEA zeolite modified by chemical and mechanochemical (M) treatments.
- Metal ions successfully incorporated via ion exchange (IE) and M methods.
- Chemical treatments created hierarchical porosity; M increased metal loading.
- Mn M incorporation gave a six-fold higher rate constant vs IE.
- Optimized BEA modification improved Fenton performance for advanced applications.

GRAPHICAL ABSTRACT

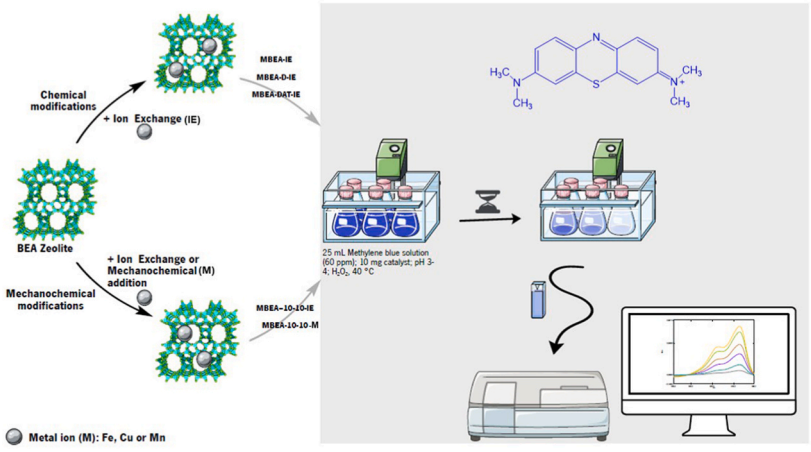

ARTICLE INFO

Keywords:
BEA zeolite
Hierarchical and mechanochemical methods

ABSTRACT

The aim of this work was to obtain improved heterogeneous Fenton catalysts with enhanced catalytic rates through modification of BEA zeolite. BEA zeolite was chosen as the support material due to its large 12-ring

* Corresponding author. Chemistry Centre of the University of Minho (CQ-UM), Department of Chemistry, University of Minho, Campus de Gualtar, 4710-057, Braga, Portugal.
E-mail address: ineves@quimica.uminho.pt (I.C. Neves).

https://doi.org/10.1016/j.matchemphys.2026.132500
Received 10 October 2025; Received in revised form 16 March 2026; Accepted 5 April 2026
Available online 6 April 2026

Metal ions
Fenton-type reaction

channels and 3D-pore network that offer favourable conditions for metal incorporation and substrate accessibility. BEA zeolite was modified through chemical desilication followed by acid treatment and, mechanochemical treatments. Fe, Cu, and Mn were introduced via two distinct methods: ion exchange and mechanochemical methods. The modified metal-ion BEA zeolites were characterized for their crystallinity, texture, and metal content, and then tested for the degradation of methylene blue using Fenton-type reactions. The reactions were monitored by UV-Vis spectroscopy, and the data were analysed with pseudo-second-order kinetic model. The results showed that the treatment methods had a strong impact on the properties of the zeolites and improved their catalytic performance. Chemical modification created hierarchical porosity on the zeolite support, while mechanochemical incorporation gave higher metal loading, especially for Mn (1.20 *vs* 0.44 wt% with ion exchange). The hierarchical FeBEA-DAT-IE catalyst showed excellent activity (k_{ap2} = 0.031 ppm^{-1} min^{-1}) and mechanochemical Mn incorporation achieved a six-fold higher rate constant than the conventional ion exchange method. Overall, this study demonstrates that rational modification of BEA zeolite can significantly enhance Fenton catalytic performance while producing materials suitable for advanced applications including potential biomedical uses.

1. Introduction

The reaction between Fe^{2+} (ferrous cation) and H_2O_2 (hydrogen peroxide) produces highly reactive hydroxyl radicals ($^{\bullet}OH$), which enable a wide range of applications, most notably the efficient degradation of pollutants in water. This process is known as the Fenton reaction [1,2]. Traditional homogenous Fenton processes use dissolved iron salts in aqueous solutions, however present several limitations including iron precipitation at neutral pH and difficulties in catalyst recovery and reuse [1]. In heterogeneous systems, iron is stabilized on solid supports, effectively addressing these challenges by allowing the generation of radicals without iron precipitation while enabling catalyst recovery [2]. When iron is replaced by other transition metals or combined with them on solid supports, the process is referred to as Fenton-type reactions [2]. These heterogeneous materials can be used in conventional water treatment [3–5] as well as in emerging biomedical applications, especially in chemodynamic therapy (CDT) [6,7].

The success of a heterogeneous Fenton catalyst largely depends on the choice of the solid support, which must provide adequate surface area, chemical stability, and accessibility to active sites. In this context, zeolite-type materials represent a significant class of inorganic materials, distinguished by their highly defined crystalline structure composed of TO_4 tetrahedral (T = Si - silicon, Al - aluminium, or other heteroatoms) [8]. The different arrangements of TO_4 result in a variety of structures, with different size of pores and channels [8]. These structures have been widely studied and used in a broad range of industrial applications, from petrochemical and environmental to agriculture and healthcare [9–11]. For Fenton applications, zeolites offer several advantages including high surface areas, tunable pore structures, excellent ion exchange capabilities, and thermal stability [9].

However, conventional zeolites often exhibit mass transfer limitations due to their microporous nature, particularly when dealing with bulky organic pollutants. Herein, several strategies have been developed to increase the catalytic activity of zeolites. Some of these strategies include the development of an additional pore system, usually mesopores, obtaining the so-called hierarchical zeolites through synthesis or post-synthesis methods [12]. Among post-synthesis methods one of the most used is desilication that consists in a selective removal of Si from the zeolite framework, using alkaline agents, being NaOH the most used. Under controlled operational conditions, the generation of intracrystalline mesoporosity occurs without severe loss of crystallinity, acidity and pristine microporosity [13,14]. Due to this treatment, the deposition of extra-framework species may occur leading to partial occlusion of the pore openings, so an additional acid leaching is recommended to remove these debris [12–15]. An alternative method is mechanochemistry, which, in the past few decades, has become a powerful tool to change the properties of zeolites by decreasing its crystal size. When compared with other methods, it also brings the advantage of being solvent-free, allowing to suppress solvent elimination and drying steps [16,17]. The intercrystalline mesoporosity resulting from the aggregation of small crystals not only improves mass transfer but also allows to explore new applications where particle size is decisive, such as in the biomedical field [16]. Furthermore, it is possible to incorporate different additives or nanoparticles during the mechanochemical process and obtain hybrid materials in a single step, with unique properties. By precisely controlling the mechanical conditions, the composition, and the distribution of these additives can be optimized, leading to materials with enhanced functionality [16–18]. However, potential drawbacks of mechanochemical procedures include heterogeneity in crystal size and the tendency for particle agglomeration. So, a careful optimization of milling parameters is needed.

Among the various zeolite frameworks, the BEA zeolite emerges as a particularly attractive candidate for Fenton applications. The large 12-ring channels and three-dimensional pore network stand out for Fenton applications since these structural characteristics provide substantial space for substrate molecules and reaction intermediates, while maintaining the crystalline order necessary for stable metal anchoring [19]. In the present work, a commercial BEA zeolite was modified using chemical or mechanical treatments, followed by the incorporation of iron (Fe^{3+}), copper (Cu^{2+}), or manganese (Mn^{2+}) ions through the classic ion exchange method or simultaneous addition of the metal ion precursors to BEA zeolite during the milling procedure. The catalytic performance was evaluated in Fenton-type reactions, focusing on the role of the intracrystalline mesoporosity, generated through chemical treatment or the intercrystalline mesoporosity due to crystal size reduction during ball milling. This comparative approach allows for a systematic evaluation of how different modification strategies affect both the structural properties and catalytic performance of BEA-based Fenton catalysts. The interpretation of the results will address two key questions: (i) can these modification methods enhance the catalytic activity in Fenton-type reaction? and (ii) which modifications yield the most effective nanomaterial for potential biomedical applications?

2. Experimental section

2.1. Modification of zeolite BEA through chemical and mechanochemical treatments

The zeolite BEA (CP814E, from Zeolyst International, SiO_2/Al_2O_3 = 25), provided in its ammonium form was modified through post-synthesis alkaline treatment (desilication), according to previously reported procedures [20], using 0.1 M NaOH (Merck, p.a) solution. The treatment was performed at 65 °C for 30 min using a liquid/solid ratio of 30 mL/g. The solid was recovered by centrifugation, washed, and dried in an oven at 110 °C. Considering that some ion exchange with sodium could occur during the alkaline treatment, the solid was re-converted to the acidic form by ion exchange with a 2.0 M NH_4NO_3 (Merck, p.a) solution using a ratio liquid/solid of 25 mL/g at 80 °C for 6 h. The recovered material was then washed, dried, and calcined for 3 h at 500 °C under dry air, being designated thereafter as BEA.

A fraction of the sample subjected to desilication was further treated with an acid wash using a 0.1 M HCl solution (Merck, p.a., fuming 37%) at 70 °C for 3 h, with a liquid-to-solid ratio of 30 mL/g. This treatment aimed to remove extra-framework aluminium species that could partially block the pore openings [14,20]. The chemically modified samples were labelled accordingly with the suffix "D" or "DAT" referring to the desilication or desilication followed by acid treatment, respectively BEA structure was also modified through mechanochemical procedures using a shaker ball mill (VWR Star-Beater). In a typical experiment, about 300 mg of dry zeolite was charged in a steel milling jar (1.5 mL capacity) with 5 steel spheres of 3 mm diameter. The sample was then milled using different times and frequencies to optimize the milling conditions. The mechanochemically modified sample was designated as BEA-X-Y, where "X" represents the frequency (Hz) and "Y" the time (min.).

2.2. Preparation of modified metal ion-BEA zeolite samples

Modified metal ion-BEA zeolite samples were prepared using two methodologies: ion exchange (IE) and mechanochemistry (M) aiming to introduce 1 wt% metal ion. The classic ion exchange was performed on parent and the modified samples obtained by chemical or mechanochemical methods, under the experimental conditions described in our previous studies [14,20,21] Therefore, the materials were mixed with 0.10 mmol of manganese ($MnCl_2.4H_2O$, Merck, p.a.), iron ($Fe(NO_3)_3.9H_2O$, Merck, p.a.), or copper ($Cu(NO_3)_2.2H_2O$, Rield-Haen, p.a.) salt solutions at room temperature during 24 h, followed by filtration, washing, drying and calcination at 350 °C for 4 h. The chemical symbol of the metal ion was added as prefix to the sample's name.

For the Mn loading through mechanochemistry, the necessary amount of $MnCl_2.4H_2O$ was introduced simultaneously with BEA on the milling jar, using the previously optimized conditions, and finally calcined using the same procedure used for the ion-exchanged samples. In the samples' designation, the metal name was added in prefix and the introduction method "IE" for ion exchange or "M" for mechanochemistry was added in the end. For example, MnBEA-10-10-M refers to BEA modified in the ball mill for 10 min at 10 Hz where the ion metal Mn was introduced through mechanochemistry. Fig. 1 represents the sample denomination according to the treatment and the type of metal addition methodology.

2.3. Characterization methods

The structural characterization of the samples was carried out using powder X-ray diffraction (Philips, Analytical PW 350/60 X'Pert PRO with X'Celerated detector). The diffractograms were acquired at room temperature using CuKα radiation as the incident beam, by continuous scanning from 5 to 40° (2θ), with a step size of 0.017° (2θ) and a time per step of 20 s. The degree of crystallinity, $C_{XRD,}$ was calculated based on the intensity of the two most intense peaks at 2θ around 8° and 22°, taking the respective parent sample as reference.

The textural characterization was made through N_2 adsorption at −196 °C using an automatic apparatus Micromeritics ASAP 2010 (Micromeritics Instruments Corporation). Prior to the isotherm measurement, the samples (around 50 mg) were outgassed at 300 °C for 3 h under vacuum $<10^{-2}$ Pa. The micropore volume, V_{micro}, and external area, A_{ext}, were quantified by applying the α_s method, taking the standard isotherm obtained for non-porous silica as reference material [22]. The V_{micro} corresponds to the back extrapolation of the linear region of α_s plot defined by the experimental points that correspond to $\alpha_s > 1$, whereas A_{ext} was calculated from the slope. The mesoporous volume, V_{meso}, was quantified from the difference between V_{total} and V_{micro}, where V_{total} is the total pore volume that corresponds to the N_2 volume adsorbed at a relative pressure of 0.95, according to the Gurvitch rule [22].

Scanning Electron Microscopy (SEM) and energy-dispersive X-ray spectroscopy (EDX) analysis were carried out on a JEOL/EO InTouchScope™ with a Super-X EDX System, operating at 200 kV to characterize BEA samples. To prevent surface charging, the samples were coated with gold under vacuum prior to analysis using a Fisons Instruments SC502 sputter coater. Transmission Electron Microscopy (TEM) analysis was performed using a JEOL JEM-2100 HT microscope operating at an

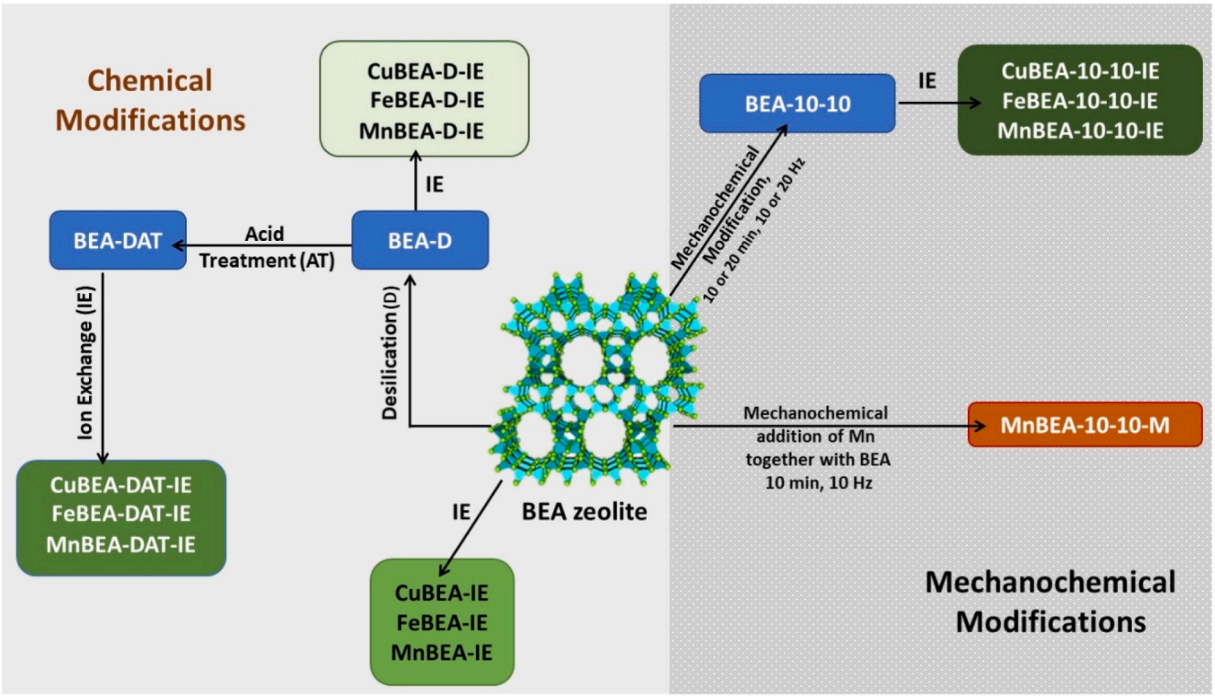

Fig. 1. Scheme of the treatments used in the preparation of the samples in this work. Note: Samples names included the metal as a prefix and the incorporation method as a suffix ("IE" for the ion exchange, "M" for the mechanochemistry). The notation BEA-X-Y was used for mechanochemically treated samples, where X and Y correspond to the milling frequency (Hz) and milling time (min), respectively.

accelerating voltage of 200 kV. The TEM micrographs were obtained using the OneView" 4k × 4k charge-coupled device (CCD) camera.

Elemental analysis was performed by inductively coupled plasma atomic emission spectroscopy (ICP-AES) for the quantification of metals in the solid samples with a 5110 ICP-OES spectrometer (Agilent Technologies), using a procedure describe in Ref. [23].

Laser light scattering (LLS) analyses were performed on a Matersizer 3000 (Malvern) for the determination of the size of crystal/crystal aggregates through wet dispersion methods, using water as dispersant. All measurements were performed in triplicate. The distribution profiles were expressed as volume distributions by applying Mie scattering theory for non-spherical particles.

X-ray photoelectron spectroscopy (XPS) analysis was performed with a Kratos Axis-Supra instrument (Thermo Fisher Scientific) using a monochromatic Mg Kα (1253.6 eV) X-ray source. Measurements were conducted in Constant Analyzer Energy (CAE) mode, including a survey spectrum with a pass energy of 150 eV and high-resolution spectra with a pass energy of 40 eV. During data processing of the XPS spectra, binding energy (BE) values were referenced to C 1 s peak (284.5 eV). ESCApe software was used for spectra treatment supplied by the manufacturer Kratos Analytical.

Fourier Transform Infrared spectroscopy (FTIR) measurements of the samples were carried out using a PerkinElmer Spectrum Two spectrometer, equipped with an ATR accessory. A diamond prism was used as the waveguide. All spectra were recorded with a resolution of 4 cm^{-1} in the wavelength region 4000-500 cm^{-1} by averaging 16 scans and the analyses were carried out at room temperature.

2.4. Catalytic activity

The catalytic performance of the samples was evaluated employing a Fenton-type reaction involving modified metal-ion BEA zeolite samples. This process was applied by using methylene blue (MB, Merck), as a model compound and monitoring its degradation over time. Briefly, seven batch experiments were prepared in 50 mL stoppered flasks with 10 mg of sample and 25 mL of 60 ppm MB solution. The flasks were immersed in a thermostatic bath at 40 °C (Julabo MP) and stirred for 60 min to reach adsorption equilibrium before starting the reaction, which is essential due to the high adsorption capacity of BEA zeolite [21]. After that, the solution pH was adjusted to 3-4 using 0.5 M HCl and the reaction was started by adding 0.5 mL of 70 mM hydrogen peroxide (H_2O_2, Merck) to only six flasks, since the seventh served as control (time zero). The reaction was stopped at intervals (5, 10, 15, 30, 45, and 60 min) by adding 50 mg of sodium thiosulfate ($Na_2S_2O_3$, Merck). The solid was separated by centrifugation at 6000 rpm for 10 min (Hermle Z206A). Supernatant aliquots were collected and their absorbances were measured by UV/vis spectroscopy using a double beam spectrophotometer (Jasco V530). Absorbance of MB was recorded in the 550-750 nm range, focusing on the MB wavelength maximum at 663 nm, using deionized water as the reference. Concentrations were determined using a calibration curve, with adjustments made for dilution to ensure compliance with the Beer-Lambert law. Each data point represents the average of at least three individual aliquots/scans, with a standard deviation below 5% to ensure data reliability.

3. Results and discussion

3.1. Characterization of BEA samples modified by chemical and mechanochemical methods

The commercial BEA structure was modified through chemical and mechanochemical treatments with dual objectives: enhancing catalytic performance through mesoporosity development obtained through chemical treatments and achieving particle sizes suitable for advanced applications by mechanochemical modifications.

For potential biomedical applications, particularly in cancer treatment, physicochemical properties such as size, shape, and surface charge are crucial, as they significantly influence the potential effectiveness and applicability of nanoparticles. These factors are emphasized in the work by Blanco et al. [24], highlighting the importance of influencing biodistribution and the ability to cross various biological barriers. Additionally, nanoparticles within the 20 to 150 nm size range demonstrated the optimal balance between effective tissue penetration and prolonged circulation times [24].

To investigate the impact of the chemical and mechanochemical treatments on the structure and texture of BEA zeolite, the samples were characterized by powder XRD and low temperature N_2 adsorption isotherms. The structural and textural characterization of the samples modified by desilication (D) or desilication followed by acid treatment (DAT), used in this study, were presented and discussed elsewhere [21], but for clarity the main properties of these samples are summarized in Table 1. Concerning the samples submitted to mechanochemistry, Fig. 2A presents the diffraction patterns and Fig. 2B displays the N_2 adsorption isotherms of parent and milled samples.

XRD results show that despite the different modifications, the samples exhibit diffractograms characteristic of the parent BEA zeolite [21, 25]. Regarding the chemically modified samples, the more significant loss of crystallinity (see Table 1) is observed upon desilication (25% loss) that only slightly increases as a consequence of acid leaching. For the mechanochemically treated materials, the grinding frequency of the ball mill seems to be the most impacting parameter since almost 50% of crystallinity is lost when 20 Hz frequency was applied (see Fig. 2A and Table 1), especially for longer grinding times, i.e. sample BEA-20-20. Sample BEA-10-10, with half frequency and time presents a small decrease in crystallinity when compared with the parent zeolite and even higher than the chemically treated samples.

The N_2 isotherms reproduced on Fig. 2A allow us to conclude that all samples present curves that can be classified as type I + IV isotherms [26]. The isotherm analysis for the chemically treated samples was presented and discussed elsewhere [21]. The correspondent textural parameters (Table 1) show for BEA-D a decrease in microporous volume (V_{micro}) that is compensated by the increase in mesoporous volume (V_{meso}), as desired. For BEA-DAT, V_{micro} is partially recovered due to the unblocking of the pore openings because of the acid leaching step. In all cases the external surface area of the crystals (A_{ext}) was identical to the parent material, suggesting that the size of the crystals or crystal aggregates was preserved. The global Si/Al ratio shows a slight decrease when compared with the pristine material that can be attributed to the

Table 1
Degree of crystallinity, (C_{XRD}), textural parameters, Al content (wt%) and Si/Al ratio. The data for parent, D and DAT samples were previously published in Ref. [21].

Sample	C_{XRD}[a] (%)	V_{micro}[b] (cm^3/g)	V_{meso}[c] (cm^3/g)	A_{ext}[b] (cm^2/g)	Al (wt %)[d]	Si/Al[d]
BEA	100	0.17	0.40	250	2.88	13.24
BEA-D	75	0.11	0.44	247	2.47	8.92
BEA-DAT	71	0.15	0.44	236	1.75	11.93
BEA-20-20	38	0.07	0.30	131	nd	nd
BEA-20-10	54	0.10	0.32	130	nd	nd
BEA-10-10	87	0.15	0.41	188	3.33	10.72

nd - not determined.

[a] Calculated from powder X-ray diffraction patterns, using parent zeolite as reference.

[b] Textural parameters calculated from N_2 adsorption isotherms at −196 °C: V_{micro} and A_{ext} applying the α_s method.

[c] V_{meso} obtained from $V_{meso} = V_{total}$-V_{micro}, being V_{total} the amount of N_2 adsorbed at $p/p^0 = 0.95$.

[d] Al content and Si/Al ratio calculated from elemental analysis.

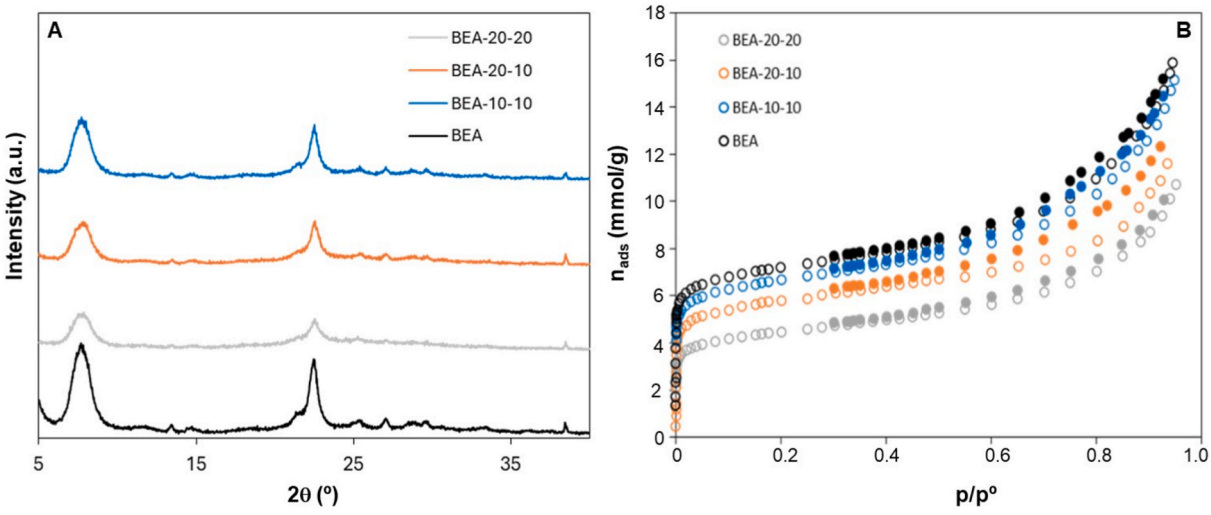

Fig. 2. XRD patterns (A) and N_2 adsorption isotherms (B) for parent and milled samples. Mechanochemically modified samples were designated BEA-X-Y, where X denotes the milling frequency (Hz) and Y the milling time (min).

removal of Si from the zeolite structure for BEA-D sample as well as extra-framework species for BEA-DAT. For the milled series in accordance with the significant loss of crystallinity, more severe grinding conditions led to the damage of the characteristic pore structure with consequent decrease of both V_{micro} and V_{meso} and an important loss of A_{ext}. On the other hand, when milder conditions were applied better preservation of textural parameters was observed for BEA-10-10 sample.

In addition, the decrease in Al content is more pronounced in the chemically treated samples. The parent BEA exhibits a Si/Al ratio of 13.24, which decreases to 8.92 after desilication (BEA-D) and subsequently increases to 11.93 following the combined desilication–acid treatment (BEA-DAT). These trends indicate the selective removal of Si during desilication, resulting in a lower Si/Al ratio for BEA-D, and the subsequent removal of extra-framework aluminium species during acid leaching, which partially restores the Si/Al ratio in BEA-DAT. Despite to have a slight decrease in Si/Al ratio for BEA-10-10 sample, the amount of Al is similar to the pristine BEA zeolite.

To investigate the modification on the size and morphology of crystal/crystal aggregates because of the chemical or mechanochemical treatments, transmission electronic microscopy (TEM) and laser light scattering (LLS) measurements were performed. Fig. 3 presents the TEM images for parent BEA zeolite with different resolutions and BEA-DAT, as an example for the chemically modified materials.

All TEM images reveal large aggregates consisting of very small crystals, a characteristic feature of BEA zeolite, as clearly seen in the TEM micrograph taken at a 50 nm scale (B). The modified sample shows some changes of the crystal aggregates, generally showing a greater level of heterogeneity. In the case of the chemically treated sample, BEA-DAT (C), the presence of some small aggregates is noted although they are not very densely stacked, with many free spaces between them. As A_{ext} is close to the one of the parent materials (see Table 1), it is assumed that the textural modifications occurred inside the zeolite crystals, as intended.

Fig. 4 shows the distribution curves expressed as volume densities as a function of the mean particle sizes. Table 2 presents the particle size data (D_{10}, D_{50} and D_{90}) along with the Span, defined as $(D_{90} - D_{10})/D_{50}$. The Span indicates the relative distance between the 10% and 90% points, normalized by the median particle size (D_{50}).

The particle size data obtained through LLS measurements complement the information given by microscopy images. For chemically treated series (Fig. 4A), the volume density profiles are practically the same, giving identical particle size data (D_{10}, D_{50} and D_{90}) and Span (Table 2), when compared with the parent BEA zeolite. On the other hand, the milled sample series profiles present some deviation especially towards larger size particles because of the denser staking, especially for BEA-20-20 sample, where high frequency and time was applied. In this case D_{90} value is significantly higher when compared to the other milled samples and, especially, the parent BEA zeolite. On the other hand, BEA-10-10 sample displays the smallest particle size parameters, with D_{10} and D_{50} slightly lower than the parent BEA zeolite. These results in addition with previous structural and textural characterization led to the selection of BEA-10-10, as the milled sample for metal incorporation and

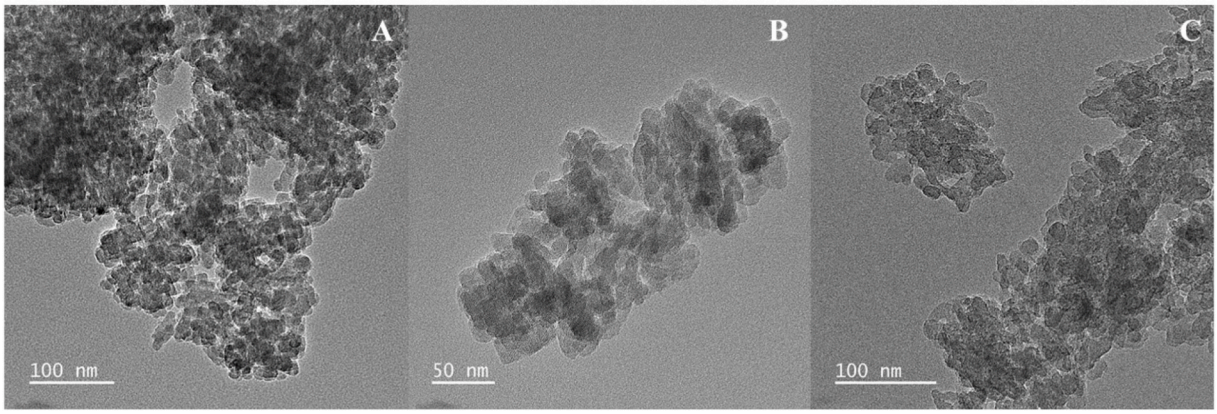

Fig. 3. TEM images with different resolutions for parent BEA (A and B) and chemically treated BEA-DAT (C).

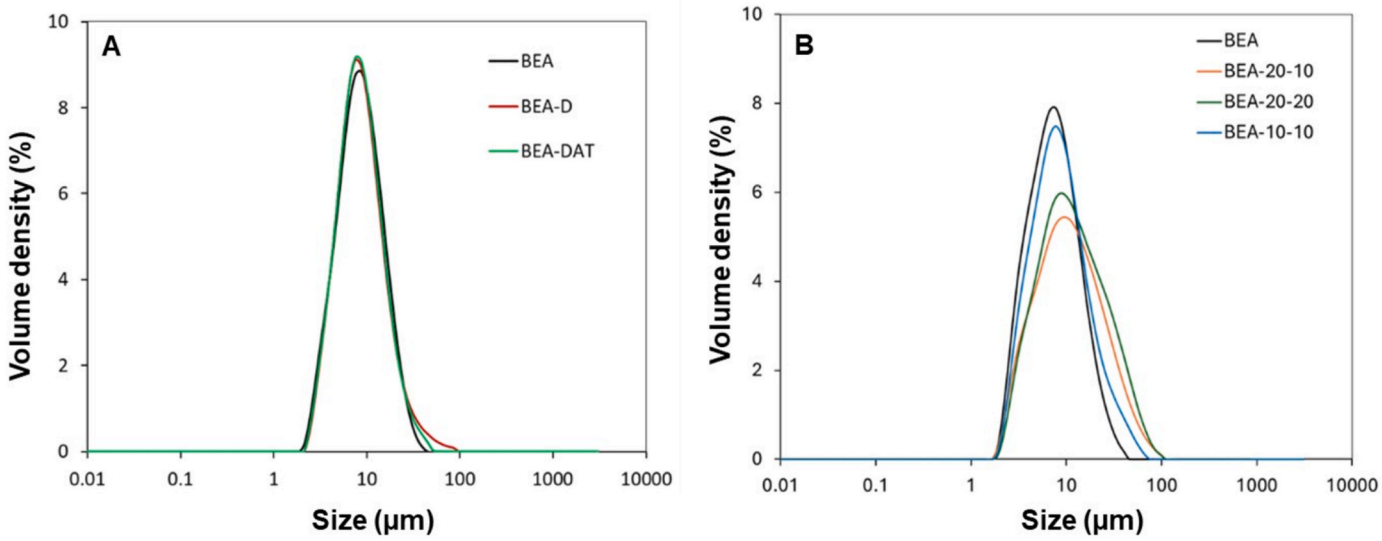

Fig. 4. Distribution of particles size determined by LLS measurements on the parent and modified samples through chemical (A) and mechanochemical (B) treatments.

Table 2
Particle size data (D_{10}, D_{50} and D_{90}) and span for parent and modified samples by chemical and mechanochemical treatments.

Sample	D_{10} (μm)	D_{50} (μm)	D_{90} (μm)	Span
BEA	4.32	8.99	18.70	1.7
BEA-D	4.49	8.93	19.90	1.7
BEA-DAT	4.44	8.87	18.70	1.6
BEA-20-20	4.09	12.2	38.3	3.5
BEA-20-10	3.81	9.06	25.5	2.3
BEA-10-10	3.77	8.63	22.9	2.2

further catalytic studies.

3.2. Characterization of modified metal-ion BEA zeolite

Metal incorporation represents a critical step in developing effective heterogeneous Fenton catalysts, as both the amount and distribution of active metal species directly influence catalytic performance. Three transition metals, Fe, Mn and Cu, were introduced in zeolite samples through ion exchange (IE) method, except for Mn which was also introduced through mechanochemistry (M) [20]. In this case, Mn salt was introduced in the milling jar with the zeolite and milled under previously optimized conditions of 10 Hz for 10 min. The presence of the metals was identified by TEM and SEM-EDX analyses (Fig. 5).

TEM images of both modified samples clearly confirm the presence of Mn, evidenced by the black spots in the micrographs, suggesting that the metal ions are located on the surface and/or within the pores (Fig. 5A, B and E). The EDX spectra of MnBEA-DAT-IE display the characteristic elements of the zeolite framework (Si, Al, and O), along with the presence of Mn (Fig. 5C). In contrast, the SEM images reveal that the mechanochemically modified sample (MnBEA-10-10-M; Fig. 5B) consists of smaller fragments compared to the chemically treated sample. However, at higher magnification (Fig. 5D, right side), the crystal aggregates appear more densely stacked, in accordance with the observed decrease in A_{ext} for the starting materials (see Table 1).

The total metal ion and aluminium content was quantified by inductively coupled plasma atomic emission spectroscopy (ICP-AES) and the surface metal content was estimated by X-ray photoelectron spectroscopy (XPS). The values are quoted on Table 3.

For parent and mechanochemical modified samples, the total metal loadings are close to the targeted value of 1 wt% for Mn, Cu, and Fe loaded samples, except for MnBEA-IE where less than half of the desired content was introduced. This reduced loading of Mn may reflect the specific coordination requirements of Mn^{2+} ions or competitive hydrolysis reactions during the exchange process. For sample FeBEA-10-10-M* the targeted value was 0.7 wt%, (see Ref. [20]). For chemically treated samples (D and DAT), the metal contents are substantially lower than the targeted value of 1 wt%, which can be attributed to some modification of the acidic properties as a consequence of the chemical treatments that impacts on the ion exchange capacity of those samples [21]. In the case of MnBEA-D-IE and MnBEA-DAT-IE, the amount of metal incorporated is only about 20% of the intended value, whereas for FeBEA-D-IE and FeBEA-DAT-IE about 80% of the desired value is incorporated, suggesting that iron exhibits stronger affinity for the modified zeolite framework or greater tolerance to the altered chemical environment created by desilication. The difference in ionic radius of the metal ions, Mn^{2+} (0.83 Å), Cu^{2+} (0.69 Å) and Fe^{3+} (0.63 Å), may explain the preferential selectivity of the BEA structure for Fe or Cu over Mn [27].

For the MnBEA and FeBEA series, the same trend observed for the parent zeolites (Table 1) is maintained, with a decrease in Al content upon chemical treatment. In contrast, for the CuBEA series, the Al content of CuBEA-D-IE and CuBEA-DAT-IE remains essentially the same amount with a slightly decrease. In addition, the results indicate that ion exchange is not complete and depends of the treatment applied, the diffusion of the metal ions and the intrinsic selectivity of the metal ions toward the zeolite framework.

The surface metal contents, probed by XPS spectroscopy for selected samples, shows that in the case of parent BEA-IE samples, the amount of metal ions Mn and Cu detected at the surface is very large, when compared with the total amount, especially in the case of Mn.

Fig. 6 displays the high-resolution XPS spectra of the photoelectron regions of the metal species present in the MnBEA-IE (A) and CuBEA-10-10-IE (B) samples, as examples.

High-resolution spectra of the Mn 2p region include four peaks at 639.1, 640.2, 643.4, and 647.4 eV for Mn 2p3/2, and two peaks at 652.8 and 654.7 eV for Mn 2p1/2, suggesting that the manganese species in BEA structure share the same oxidation state.

The major contribution in the Mn 2p3/2 broad band deconvoluted in four peaks is the peak at 640.2 eV (20%) followed by 643.4 eV (18%) for MnBEA-IE. These BE values are probably typical of manganese cations in the oxidation state (II) or (IV), according to the NIST XPS database and the literature [28–30]. The presence of both oxidation states in these

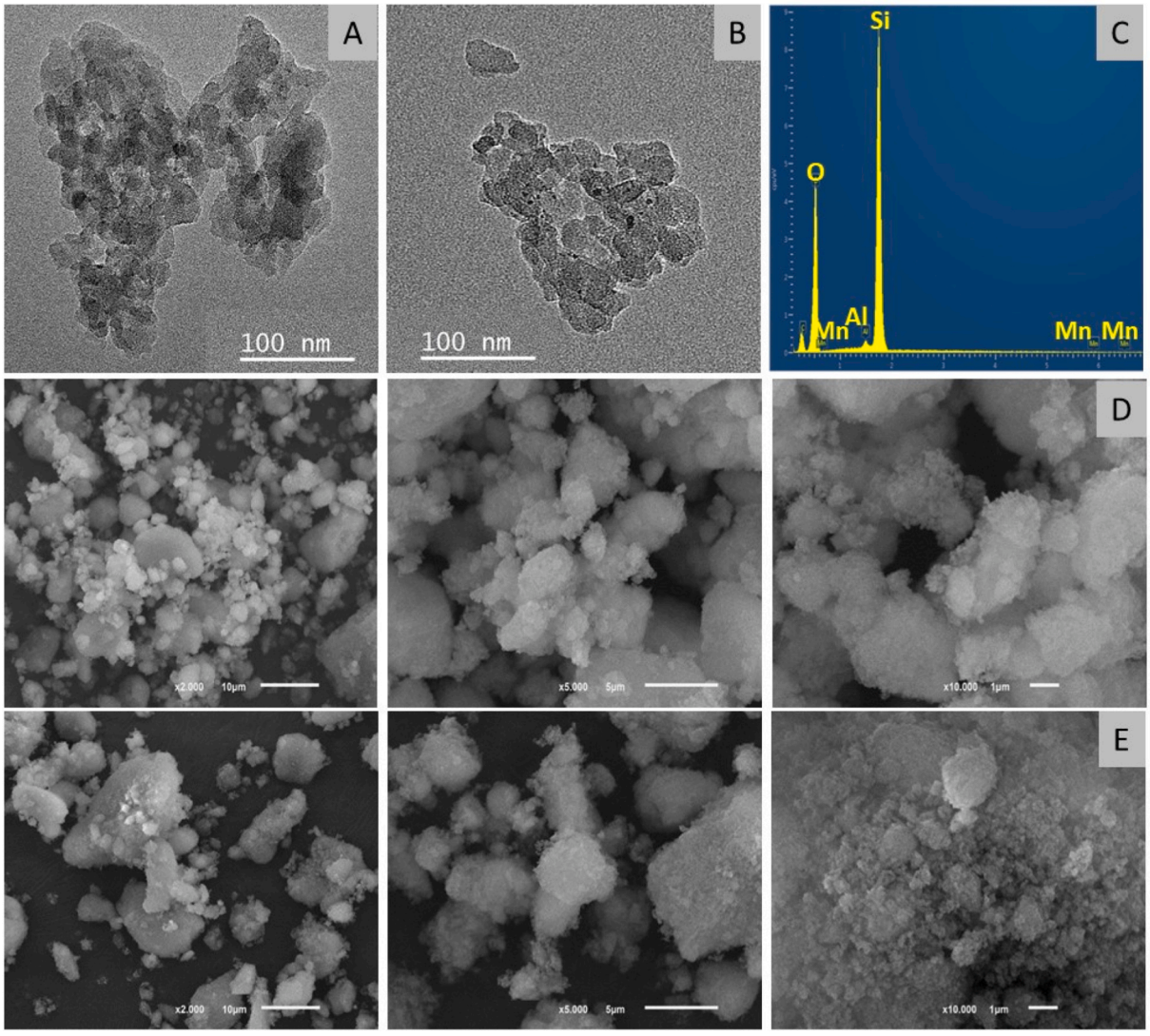

Fig. 5. TEM images of MnBEA-DAT-IE (A) and MnBEA-10-10-M (B) samples; EDX spectra of MnBEA-DAT-IE (C); SEM images of chemically treated CuBEA-DAT (D) and mechanochemically modified MnBEA-10-10-M (E) samples.

Table 3
Metal contents quantified by ICP-AES and XPS (values in bold). For "*" sample, value from Ref. [20]. Note: Metal names were added as prefixes, while suffixes indicated the incorporation method: IE – ion exchange, M – mechanochemistry.

Sample	Metal content (*wt.*% and mmmol)							
	Al		Mn		Cu		Fe	
	(wt%)	(mmol)	(wt%)	(mmol)	(wt%)	(mmol)	(wt%)	(mmol)
MnBEA-IE	2.88	1.04	0.44 **(0.40)**	0.080	-	-	-	-
MnBEA-D-IE	2.47	0.84	0.08	0.015	-	-	-	-
MnBEA-DAT-IE	1.75	0.57	0.20	0.018	-	-	-	-
MnBEA-10-10-IE	3.33	1.04	0.56	0.100	-	-	-	-
MnBEA-10-10-M	2.81	0.87	1.20	0.220	-	-	-	-
CuBEA-IE	2.45	0.91	-	-	0.93 **(0.76)**	0.15	-	-
CuBEA-D-IE	2.22	0.82	-	-	0.50	0.08	-	-
CuBEA-DAT-IE	2.00	0.74	-	-	0.40	0.06	-	-
CuBEA-10-10-IE	1.85	0.69	-	-	0.83 (**0.11**)	0.13	-	-
FeBEA-IE	2.47	0.92	-	-	-	-	1.06	0.19
FeBEA-D-IE	1.83	0.68	-	-	-	-	0.77 (**0.26**)	0.14
FeBEA-DAT-IE	1.50	0.56	-	-	-	-	0.85 (**0.43**)	0.15
FeBEA-10-10-IE	1.92	0.71	-	-	-	-	1.05	0.19
FeBEA-10-10-M*	-	-	-	-	-	-	0.65	-

zeolites is attributed to their higher Si/Al ratio, alongside a lower concentration of manganese ions, as proposed in other studies [29,30].

The high-resolution spectrum of the Cu 2p region for CuBEA-10-10-IE shows a poor peak fit, suggesting that the metal is predominantly

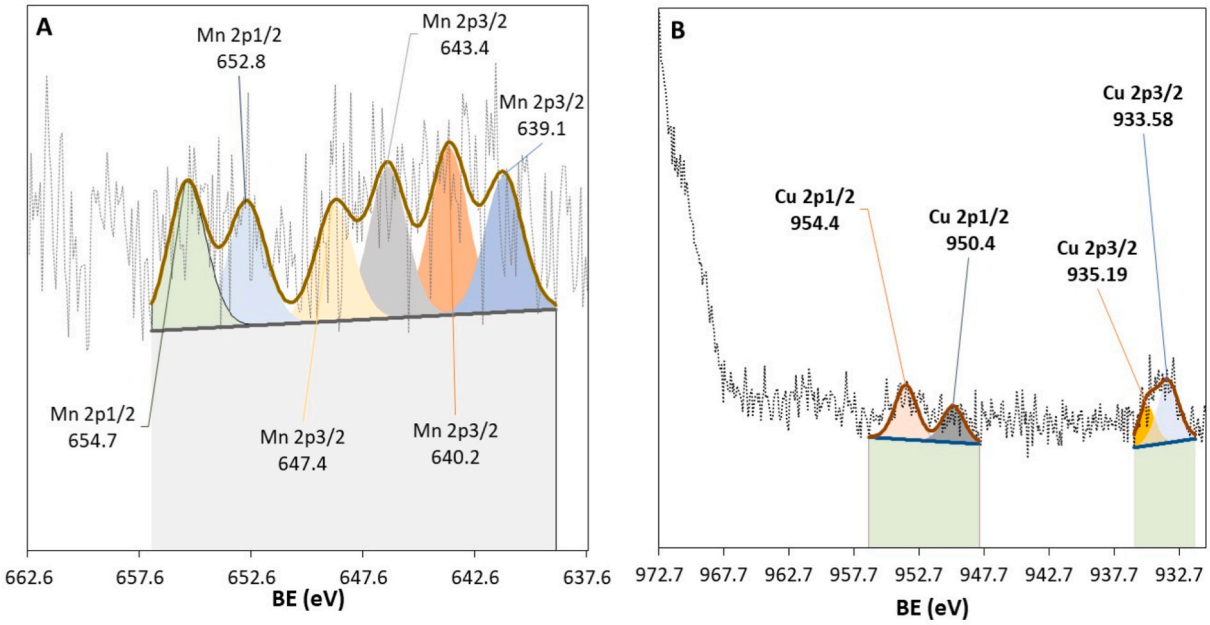

Fig. 6. High XPS spectra of Mn and Cu photoelectron regions from MnBEA-IE (A) and CuBEA-10-10-IE (B).

located within the zeolite structure. However, the contributions of the two peaks in both Cu 2p3/2 and Cu 2p1/2 regions are similar, with each accounting for approximately 50%. The largest contribution within the Cu 2p3/2 doublet is 33.5% at 933.58 eV, while for Cu 2p1/2, it is 30% at 953.74 eV values that are consistent with the oxidation state of copper (II) [28,31,32]. Finally, in the high-resolution Fe 2p spectra of both iron-BEA samples, five distinct peaks are identified, two for Fe 2p1/2 and three for Fe 2p3/2 regions. The BE values identified, in accordance with the NIST XPS database and the literature, indicate that the surface Fe is associated with ferric ions (Fe^{3+}) [28,29,33].

XPS analysis revealed surface metal concentrations that differed from the total metal contents determined by ICP-AES, highlighting the heterogeneous distribution of metals within the zeolite framework and the influence of the preparation method. Specifically, MnBEA-IE exhibited a Mn surface concentration of 0.40 wt%, while CuBEA-10-10-IE showed 0.11 wt% Cu, indicating that the synthesis approach strongly affects the distribution of metals within the pore structure. For Mn-BEA-IE, 91% of the total amount of Mn is located near the surface, as well as 82% of Cu is on the surface in the CuBEA-IE sample (see Table 3). Remarkably, for CuBEA-10-10-IE, the textural and morphological modification made by the mechanochemical treatment allowed an effective diffusion of the Cu inside the pores since only about 13 % of the total Cu amount is located at the external surface. Nevertheless, this was not observed for the FeBEA-D-IE and FeBEA-DAT-IE samples, in which only 34% and 51%, respectively, of the total Fe was located on the external surface, while the remainder was successfully exchanged into the pore structure. This behaviour contrasts sharply with the high surface metal concentrations observed for MnBEA-IE and CuBEA-IE. The development of mesoporosity induced by chemical treatments positively affected metal ion diffusion within the zeolite pore network during ion exchange. In the mechanochemically modified samples, the reduced size of the milled crystal aggregates shortened the diffusion path length, thereby explaining the enhanced metal loading (Table 3). Moreover, these samples exhibited a pronounced shift in surface versus internal metal distribution; for example, CuBEA-10-10-IE contained only 13% surface Cu compared to 82% for CuBEA-IE.

In order to understand if all metal ion species are ion exchanged in BEA framework, FTIR analysis was performed with BEA, MnBEA-IE, CuBEA-IE and FeBEA-IE (Fig. S1a)) and the modified samples (Fig. S1b) and c)).

The BEA zeolite spectrum in the 3750–3000 cm^{-1} region shows distinct ν(OH) vibrations at 3650 cm^{-1} and a broad band in the 3600–3000 cm^{-1} range. These bands are attributed to OH groups associated with extra-framework or partially extra-framework Al species and to hydrogen-bonded silanols or hydrogen-bonded framework-bridged OH groups (Si–OH–Al sites), respectively [34–37]. The T–O–T vibrational bands, characteristic of framework Si–O or Al–O bonds, appear in the regions 1000–1300 cm^{-1} and 620–800 cm^{-1}, corresponding to asymmetric and symmetric stretching vibrations, respectively [34–37]. The band at 1470 cm^{-1} is likely associated with the presence of NH_4^+ ions acting as counterions in the zeolite framework [37], (Table S1).

The metal-modified samples exhibit the typical bands of BEA zeolite, confirming that the parent framework structure is preserved after metal incorporation. After the introduction of metal ions in BEA zeolite, the intensity of the broad band 3600-3000 cm^{-1} decreased and the band at 1470 cm^{-1} disappeared, which confirms that these sites have ion exchange capacity [37]. These changes indicate that the ion exchange with metal ions occurred successfully, suggesting an overall ion-exchange process within the zeolite structure.

For both the chemically and mechanochemically modified samples, the same spectral pattern was observed for all materials, although a reduction in the intensity of the characteristic BEA zeolite bands was noted, as is evidenced in the spectra of the CuBEA series, as example (Fig. S1b) and c)).

3.3. Heterogeneous Fenton reaction

The degradation of methylene blue (MB) was performed by heterogeneous Fenton or Fenton-type reaction. MB, a dye from the phenothiazine family, was selected as a model molecule to study degradation behaviour of the samples [20]. The temperature (40 °C) and pH (3.0) were set based on the optimal values identified in a preliminary study conducted in a semi-batch reactor under atmospheric pressure and stirring [10,38,39]. Similarly, the catalyst mass (0.4 g/L), hydrogen peroxide concentration (70 mM), and the equilibrium step of, at least 1 h of contact between the samples and MB to isolate the catalytic performance from the initial adsorption phenomena, was previously optimized [20]. In addition, to investigate possible influence of parent and starting zeolite samples (without ion metal loadings) control experiments were

made. In the sole presence of H_2O_2, a negligible MB conversion was noted, meaning that the reaction is only effective in the presence of the heterogeneous catalysts.

Fig. 7 presents the kinetic curves for the degradation of MB over a 60-min reaction period in the presence of Mn, Cu and Fe-BEA prepared samples. To compare quantitatively the catalytic performance, kinetic constants were calculated from the observed kinetic using pseudo-second-order (Eq. (1)) model, since previous studies demonstrated that this model offers a closer description of Fenton reaction kinetics as it allows to capture the interaction between reactive species and the catalyst [38,39].

$$\frac{[C]}{[C_0]} = \frac{1}{[C_0](k_{ap2}t) + 1} \quad \text{(Eq. 1)}$$

where $[C]$ is the dye concentration, $[C_0]$ is the initial dye concentration, k_{ap2} is the pseudo-second order constant and t is the reaction time.

The numerical results of the kinetic constants, determined using Table Curve 2D 5.0 software, are presented in Table 4 as well as the statistical parameters for the non-linear regression *i.e.* coefficient of determination (R^2), fit standard error of the regression (s_{Fit}), Fisher-

Table 4
Pseudo-second-order model applied to MB degradation: kinetic constant ($\boldsymbol{k_{ap2}}$) and statistical parameters for the nonlinear regression. The data for sample "*" are quoted from Ref. [20].

Sample	k_{ap2} ($ppm^{-1}\ min^{-1}$)	R^2	s_{Fit}	F	N
MnBEA-IE	0.0021 ± 0.0003	0.936	0.0643	72.7	7
MnBEA-D-IE	0.0008 ± 0.0001	0.948	0.0496	60.3	6
MnBEA_DAT-IE	0.0010 ± 0.0002	0.923	0.0776	60.3	6
MnBEA-10-10-IE	0.0012 ± 0.0002	0.897	0.0640	43.6	6
MnBEA-10-10-M	0.0069 ± 0.0010	0.922	0.0644	47.6	5
CuBEA_IE	0.0049 ± 0.0040	0.974	0.0400	183.7	6
CuBEA-D-IE	0.0013 ± 0.0001	0.941	0.0382	64.1	5
CuBEA-DAT-IE	0.0008 ± 0.0001	0.945	0.0518	68.8	5
CuBEA-10-10-IE	0.0230 ± 0.0030	0.975	0.0530	198	6
FeBEA_IE	0.0070 ± 0.0010	0.971	0.0665	134.1	5
FeBEA-D-IE	0.0008 ± 0.0001	0.977	0.0280	211.9	6
FeBEA-DAT-IE	0.0310 ± 0.0020	1.000	0.0062	19593.5	6
FeBEA-10-10-IE	0.0043 ± 0.0009	0.947	0.0879	88.8	6
FeBEA-10-10-M*	0.0034 ± 0.0006	0.953	0.0740	79.0	5

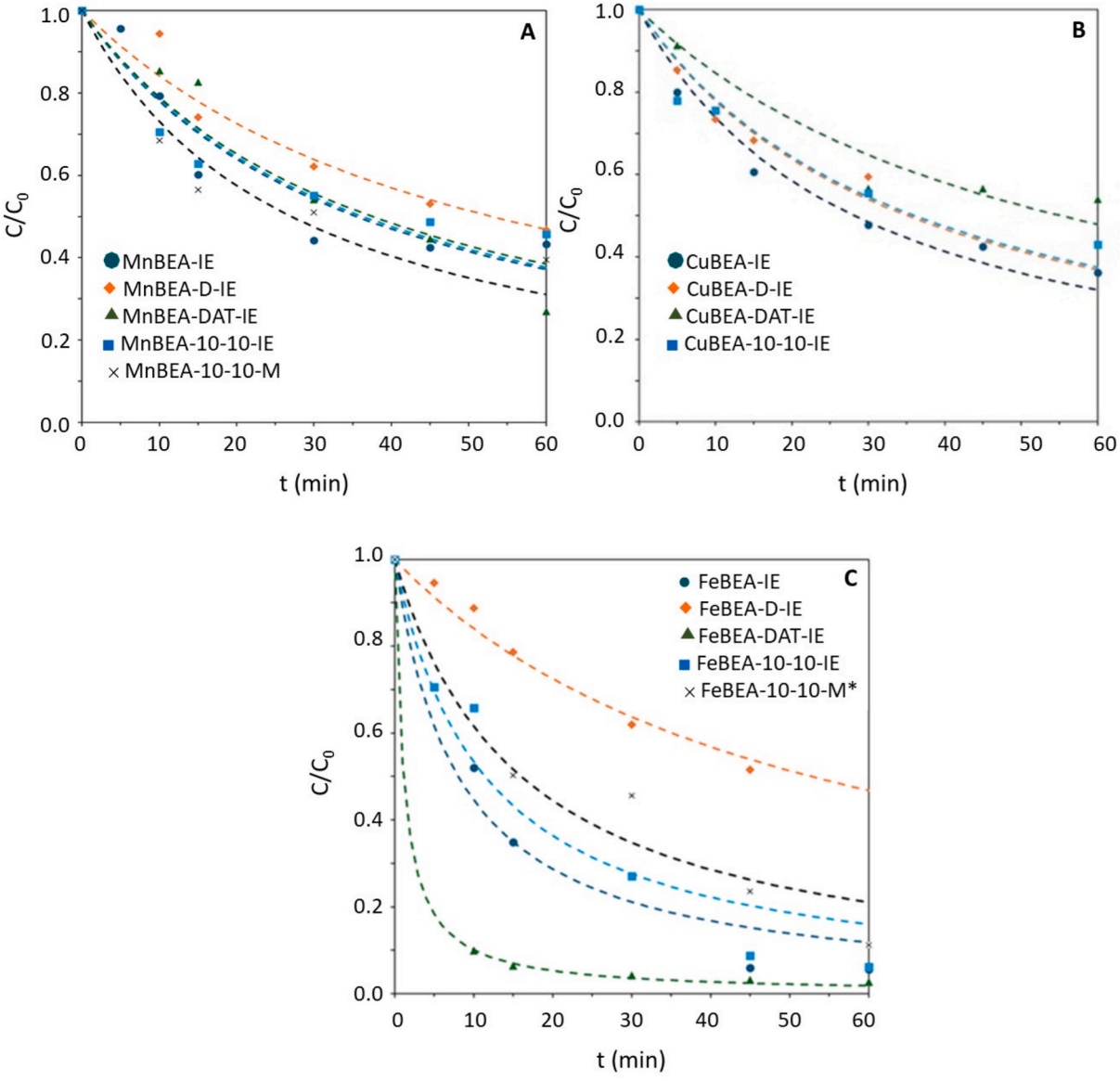

Fig. 7. MB degradation kinetic curves for MnBEA series (A), CuBEA series (B) and FeBEA series (C). The markers denote the experimental values and the dashed lines correspond to pseudo-second-order model. FeBEA-10-10-M* sample from Ref. [20].

Snedecor parameter (*F*) and the number of data points used (*N*).

As anticipated from the fundamental Fenton chemistry principle, Fe-loaded samples demonstrated superior catalytic performance compared to Cu and Mn analogues, reflecting Fe's well-established role as effective metal for •OH generation [10,27,38,39]. This can be partially attributed to the higher ion metal content of the Fe loaded samples, as confirmed by ICP-AES analysis (Table 3), In fact, the amount of ion metals is, in general, well correlated with the obtained rate constants as can be observed in Fig. 8. However, there are some outliers, precisely on Fe loaded samples, suggesting that the characteristics of the zeolite support may have some influence.

As can be seen on Fig. 7C, the chemically treated sample, FeBEA-DAT-IE shows the highest catalytic efficiency, especially in the first 10 min reaction. By contrast, the other chemically treated sample FeBEA-D-IE shows the worst performance compared to all samples of FeBEA series, these correspond to the two-outlier points in Fig. 8. Considering that, these samples contain similar amount of ion metal and the XPS analysis reveal that a large amount of it is inside the zeolite porous structure; this opposite behaviour can only be attributed to the characteristics of the zeolite support. In fact, the desilicated sample FeBEA-D-IE shows a decrease in V_{micro} (see Table 1) due to partial pore blockage by the debris formed as a consequence of the alkaline treatment [21]. Therefore, despite that no limitations occur in the diffusion of Fe ions during the ion exchange, the same is not true for the voluminous MB molecule, slowing the catalytic reaction, as seen on Fig. 7C and by the low value of the rate constant on Table 4. On the other hand, for FeBEA-DAT-IE, the acid washing after alkaline treatment removes the debris, allowing some recovery of V_{micro} that, allied to an easier diffusion promoted by the mesopores, which improves the access of MB to the ion metal sites located inside the micropores.

For zeolites modified by mechanochemistry followed by ion exchange, higher amounts of metal ions are generally introduced compared to the parent and chemically modified counterparts. This enhancement can improve the catalytic efficiency, which is attributed to the facilitated access of MB molecules to the internal active sites, as the reduced size of the milled crystal aggregates shortens the diffusion pathway. It must be emphasized that the simultaneous introduction of the zeolite and metal ion precursors in the ball mill resulted in improved catalytic efficiency, especially for MnBEA-10-10-M, where the amount of Mn introduced is two times higher when compared with IE method, resulting in a rate constant gain of almost six times. On the other hand, for Fe samples in the same conditions, a decrease of about 40% in the ion metal content led to a solely reduction of the rate constant from 0.0043 to 0.0034 ppm^{-1} min^{-1} (about 20 %).

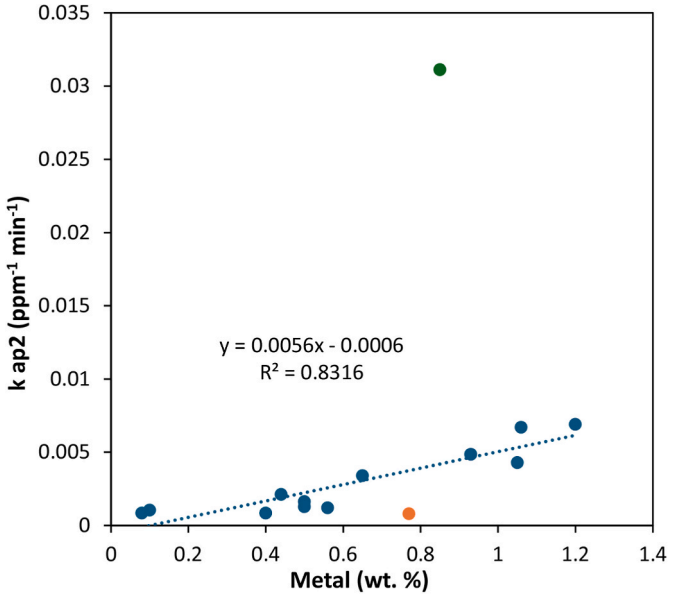

Fig. 8. Pseudo-second-order rate constants as a function of the total amount of loaded metal ions.

The choice of metal precursors was guided by their well-established suitability for zeolite ion exchange. During the ion exchange process, these cations replace charge-compensating species associated with the anionic zeolite framework. The higher charge density of Fe^{3+} compared to Cu^{2+} and Mn^{2+} likely results in stronger electrostatic interactions with framework sites, which is consistent with the higher and uniform Fe loadings observed across the different samples. With respect to catalytic performance, the presence of Fe^{3+} aligns with classical Fenton chemistry, in which the Fe^{3+}/Fe^{2+} redox cycle enables efficient generation of •OH radicals, responsible for the degradation of the MB molecules. In contrast, Cu^{2+} and Mn^{2+} participate in Fenton-type mechanisms. These systems are generally more sensitive to metal dispersion, coordination environment, and accessibility, which is reflected in their catalytic behaviour [10,19]. Notably, mechanochemical incorporation of Mn resulted in a six-fold increase in the rate constant compared to conventional ion exchange (Table 4), while the improved internal distribution of Cu in mechanochemically modified zeolites led to an almost five-fold enhancement in activity (Table 4). This pronounced dependence on preparation method for Cu- and Mn-based catalysts highlights the importance of optimizing both the metal incorporation strategy and the support structure in Fenton-type catalytic systems.

Catalyst stability and reusability have been previously evaluated for analogous metal-zeolite systems prepared using similar methodologies in this study [20]. In that work, iron-loaded zeolite catalysts prepared through both ion exchange and mechanochemical methods demonstrated high degradation efficiency (85-95%) over two consecutive catalytic cycles, confirming good reusability. For the third cycle, the degradation efficiency reduced significantly due to progressive iron leaching, however control studies with Fe^{3+} in solution with concentrations equivalent to the zeolite iron content demonstrated that leached iron contributes negligibly to methylene blue degradation. These results validate the practical stability and predominantly heterogeneous nature of metal-loaded zeolite catalysts prepared through methodologies employed in the current study. Future work will focus on stability and reusability evaluations of specific catalysts identifies in this study, particularly FeBEA-DAT-IE and the high-loading MnBEA-10-10-M samples, to establish their long-term performance characteristics and optimize regeneration protocols.

Throughout this study, two main questions were addressed: *(i) Can these modification methods enhance the catalytic activity in Fenton-type reaction?* The results demonstrate that enhancement in the catalytic performance can be achieved through the optimal combination of high metal content, increased mesoporosity, and adequate crystallinity. Overall, chemically modified BEA zeolite with metal incorporation through ion exchange showed lower metal loading and rate constants when compared to the pristine metal-loaded BEA zeolite, except for FeBEA-DAT-IE, which exhibited an exceptional rate constant (0.031 ppm^{-1} min^{-1}). This superior performance can be explained by the combination of the high iron content and the favourable textural characteristics of modified BEA zeolite. Indeed, the hierarchical structure of FeBEA-DAT-IE sample exhibited increased micropore and mesopore volumes, allowing better diffusion of MB molecules to the active metal sites located within the pore network. Mechanochemically modified BEA zeolite with co-incorporation of metal species showed superior metal loading and increased rate constants, particularly evident for samples containing manganese. MnBEA-10-10-M sample showed a 2.7-fold increase in metal loading and a 6-fold enhancement in rate constant when compared to the conventional ion exchange method applied to mechanochemically modified BEA zeolite.

(ii) *Which modifications yield the most effective nanomaterial for potential biomedical applications?* To answer this, several factors should be considered: the metal content, the metal accessibility, and the physical characteristics of the resulting materials. Regarding metal accessibility, it should be noted that metals present at external surfaces are more susceptible to leaching, potentially reducing long-term stability. Concerning physical alterations, mechanochemically modified samples showed a decreased external surface area and exhibited more densely packed structures. This densification presents both advantages and challenges for biomedical applications: while the reduced particle size falls within the optimal range for biological systems (20 – 150 nm), the increased density may affect dispersibility in aqueous media. However, mechanochemically modified samples show promising improvements in terms of catalytic performance, combined with favourable particle size distributions, making them viable candidates for potential biomedical applications. The enhanced metal loading efficiency and superior catalytic activity, particularly demonstrated by manganese-containing samples, position these materials as promising platforms for CDT applications where controlled radical generation is essential.

4. Conclusions

Successful modifications of BEA zeolite were achieved through chemical and mechanochemical treatments, followed by the incorporation of transition metals (Fe, Cu, Mn) via ion-exchange and mechanochemical methods. These modifications showed enhanced catalytic activity in Fenton-type reactions, with mechanochemical co-incorporation, particularly of Mn, yielding the highest metal loading and rate constants. While chemically modified samples were generally less efficient, FeBEA-DAT-IE stood out due to its high Fe content and hierarchical structure. These results are quite promising since the combination of two positive effects results in the production of more effective Fenton heterogeneous catalysts: (i) the preparation of metal loaded catalyst in ball mill waives the use of solvents and further drying steps, which is particularly relevant in large-scale processes; (ii) mechanochemically modified samples also exhibited favourable particle sizes for biomedical use, positioning Mn-BEA zeolite samples as promising candidates for biomedical applications.

CRediT authorship contribution statement

V. Ivasiv: Writing – original draft, Investigation, Formal analysis. **A. R. Bertão:** Writing – original draft, Investigation, Formal analysis. **A. Martins:** Writing – review & editing, Validation, Supervision, Investigation. **N. Nunes:** Writing – review & editing, Validation, Supervision, Investigation. **A.P. Carvalho:** Writing – review & editing, Validation, Supervision, Investigation. **A.M. Fonseca:** Writing – review & editing, Funding acquisition. **E. Rombi:** Writing – review & editing, Validation, Investigation. **J.N. Moreira:** Writing – review & editing, Validation, Supervision. **F. Baltazar:** Writing – review & editing, Validation, Supervision. **I.C. Neves:** Writing – review & editing, Validation, Supervision, Project administration, Funding acquisition, Conceptualization.

Declaration of competing interest

The authors declare that they have no known competing financial interests or personal relationships that could have appeared to influence the work reported in this paper.

Acknowledgements

V.I. acknowledges the financial support from Portuguese Foundation for Science and Technology (FCT, Portugal) through the PhD fellowship UI/BD/152219/2021. FCT supported this work in the framework of the Strategic Funding projects: Centre of Chemistry of the University of Minho (CQ-UM/UM, UID/0686/2025 research unit, https://doi.org/10.54499/UID/00686/2025), Centre of Biological Engineering of the University of Minho (CEB, UID/04469/2025 research unit, https://doi.org/10.54499/UID/04469/2025), ICVS (UIDP/50026/2020), CQE (UIDB/00100/2020), and the Instituto Politecnico de Lisboa (IPL), through Project IPL/2022/ZeoMed ISEL.

Appendix A. Supplementary data

Supplementary data to this article can be found online at https://doi.org/10.1016/j.matchemphys.2026.132500.

Data availability

Data will be made available on request.

References

[1] H.J.H. Fenton, LXXIII.—Oxidation of tartaric acid in presence of iron, J. Chem. Soc. Trans. 65 (1894) 899–910, https://doi.org/10.1039/CT8946500899.
[2] Y. Liu, Y. Zhao, J. Wang, Fenton/Fenton-like processes with in-situ production of hydrogen peroxide/hydroxyl radical for degradation of emerging contaminants: advances and prospects, J. Hazard. Mater. 404 (2021) 124191, https://doi.org/10.1016/j.jhazmat.2020.124191.
[3] A.R. Ribeiro, O.C. Nunes, M.F.R. Pereira, A.M.T. Silva, An overview on the advanced oxidation processes applied for the treatment of water pollutants defined in the recently launched directive 2013/39/EU, Environ. Int. 75 (2015) 33–51, https://doi.org/10.1016/j.envint.2014.10.027.
[4] A.G. Trovó, T.F.S. Silva, O. Gomes Jr., A.E.H. Machado, W. Borges Neto, P. S. Muller Jr., D. Daniel, Degradation of caffeine by photo-Fenton process: optimization of treatment conditions using experimental design, Chemosphere 90 (2013) 170–175, https://doi.org/10.1016/j.chemosphere.2012.06.022.
[5] A. Šuligoj, M. Grilc, B. Likozar, U. Novak Tušar, Bimetal Cu-Mn porous silica-supported catalyst for Fenton-like degradation of organic dyes in wastewater at neutral pH, Catal. Today 358 (2020) 270–277, https://doi.org/10.1016/j.cattod.2020.03.047.
[6] Z. Tang, Y. Liu, M. He, W. Bu, Biomedicine meets fenton chemistry, Chem. Rev. 121 (2021) 1981–2019, https://doi.org/10.1021/acs.chemrev.0c00977.
[7] L. Yang, H. Yang, S. Yin, X. Wang, M. Xu, G. Lu, Z. Liu, H. Sun, Fe single-atom catalyst for efficient and rapid fenton-like degradation of organics and disinfection against bacteria, Small 18 (2022) 2104941, https://doi.org/10.1002/smll.202104941.
[8] J. Cejka, H. Van Bekkum, Zeolites and ordered mesoporous materials: progress and prospects, in: Studies in Surface Science and Catalysis, vol. 157, Elsevier, Amsterdam, 2005.
[9] Q. Zhang, S. Gao, J. Yu, Metal sites in zeolites: synthesis, characterization, and catalysis, Chem. Rev. 123 (2022) 6039–6106, https://doi.org/10.1021/acs.chemrev.2c00315.
[10] O. Assila, Ó. Barros, A.M.F. Fonseca, P. Parpot, O.S.G.P. Soares, M.F.R. Pereira, F. Zerrouq, A. Kherbeche, E. Rombi, T. Tavares, I.C. Neves, Degradation of pollutants in water by Fenton-like oxidation over LaFe-catalysts: optimization by experimental design, Microporous Mesoporous Mater. 349 (2023) 112422, https://doi.org/10.1016/j.micromeso.2022.112422.
[11] M.K. Yazdi, P. Zarrintaj, A. Akbari, M.R. Saeb, N. Yousefi, Zeolites for theranostic applications, J. Mater. Chem. B 8 (2020) 5992–6012, https://doi.org/10.1039/D0TB00719F.
[12] A.P. Carvalho, N. Nunes, A. Martins, Hierarchical zeolites: preparation, properties and catalytic applications, in: Comprehensive Guide for Mesoporous Materials, Properties and Development, ume 3, Nova Science Publisher Inc., New York, 2015, pp. 147–211.
[13] A. Martins, N. Nunes, A.P. Carvalho, P.M. Lourenço, M. Pires, Friedel-crafts acylation reaction over hierarchical Y zeolite modified through surfactant mediated technology, Microporous Mesoporous Mater. 323 (2021) 111167, https://doi.org/10.1016/j.micromeso.2021.111167.
[14] N. Nunes, A. Martins, A.P. Carvalho, R. Neves, C. Henriques, Exploring the effect of hierarchical porosity in BEA zeolite in friedel-crafts acylation of furan and benzofuran, Catalysts 12 (2022) 1064, https://doi.org/10.3390/catal12091064.
[15] J.D.G. da Rocha, A.F. Cunha, M.C. Hernandes, P.T.C. Freire, A.G.S. Prado, Advances and environmental aspects on the synthesis of hierarchical zeolites revisited: a state-of-the-art description, J. Environ. Chem. Eng. 11 (2023) 109397, https://doi.org/10.1016/j.jece.2023.109397.
[16] G. Majano, L. Borchardt, S. Mitchell, V. Valtchev, J. Pérez-Ramírez, Rediscovering zeolite mechanochemistry–A pathway beyond current synthesis and modification boundaries, Microporous Mesoporous Mater. 194 (2014) 106–114, https://doi.org/10.1016/j.micromeso.2014.04.006.
[17] D.N. Rainer, R.E. Morris, New avenues for mechanochemistry in zeolite science, Dalton Trans. 50 (2021) 8995–9009, https://doi.org/10.1039/D1DT01440D.
[18] K. Akçay, I.E. Wachs, H. Balci, Wet ball milling of zeolite HY, Powder Technol. 142 (2004) 121–128, https://doi.org/10.1016/j.powtec.2004.03.012.

[19] L. Ye, A. Chica, F. Thibault-Starzyk, F. Schüth, The influence of pore-architecture over n-heptane cracking using MFI, BEA and MSE zeolite catalysts: multipore versus hierarchical porosity, Chem. Eng. J. 482 (2024) 148705, https://doi.org/10.1016/j.cej.2024.148705.
[20] A.P. Carvalho, J. Costa, A. Martins, A.M. Fonseca, I.C. Neves, N. Nunes, Zeolite modification for optimizing Fenton reaction in methylene blue dye degradation, Colorants 4 (2025) 10, https://doi.org/10.3390/colorants4010010.
[21] R. Aleixo, R. Elvas-Leitão, F. Martins, A.P. Carvalho, A. Brigas, R. Nunes, A. Fernandes, J. Rocha, A. Martins N. Nunes, Zooming in with QSPR on Friedel-crafts acylation reactions over modified BEA zeolites, Mol. Catal. 476 (2019) 110495, https://doi.org/10.1016/j.mcat.2019.110495.
[22] S.J. Gregg, K.S.W. Sing, Adsorption, Surface Area and Porosity, Academic Press, London, 1982.
[23] P. Peixoto, M. Costa, A.M. Fonseca, I.C. Neves, Metal ion–zeolite materials against resistant bacteria, MRSA, Ind. Eng. Chem. Res. 60 (2021) 12883–12892, https://doi.org/10.1021/acs.iecr.1c01736.
[24] E. Blanco, H. Shen, M. Ferrari, Principles of nanoparticle design for overcoming biological barriers to drug delivery, Nat. Biotechnol. 33 (2015) 941–951, https://doi.org/10.1038/nbt.3330.
[25] M.M. Treacy, J.B. Higgins, Collection of Simulated XRD Powder Patterns for Zeolites Fifth (5Th) Revised Edition, Elsevier, Amsterdam, 2007.
[26] M. Thommes, K. Kaneko, A.V. Neimark, J.P. Olivier, F. Rodriguez-Reinoso, J. Rouquerol, K.S.W. Sing, Physisorption of gases, with special reference to the evaluation of surface area and pore size distribution (IUPAC technical report), Pure Appl. Chem. 87 (2015) 1051–1069, https://doi.org/10.1515/pac-2014-1117.
[27] E.A. Permyakov, Metal binding proteins, Encyclopedia 1 (2021) 261–292, https://doi.org/10.3390/encyclopedia1010024.
[28] A. Naumkin, A.V. Kraut-Vass, S.W. Gaarenstroom, C.J. Powell, A.Y. Lee, NIST X-ray Photoelectron Spectroscopy Database, vol.20, NIST Standard Reference Database, 2023, https://doi.org/10.18434/T4T88K. Version 5.0, Last Update to Data Content.
[29] J.C. Carver, G.K. Schweitzer, T.A. Carlson, Use of X-ray photoelectron spectroscopy to study bonding in Cr, Mn, Fe, and Co compounds, J. Chem. Phys. 57 (1972) 973–982, https://doi.org/10.1063/1.1678348.
[30] I.K. Biernacka, A.M. Fonseca, I.C. Neves, Manganese complexes with triazenido ligands encapsulated in NaY zeolite as heterogeneous catalysts, Inorg. Chim. Acta. 394 (2013) 591–597, https://doi.org/10.1016/j.ica.2012.09.027.
[31] D.C. Frost, A. Ishitani, C.A. McDowell, X-ray photoelectron spectroscopy of copper compounds, Mol. Phys. 24 (1972) 861–877, https://doi.org/10.1080/00268977200101961.
[32] P. Parpot, C. Teixeira, A.M. Almeida, C. Ribeiro, I.C. Neves, A.M. Fonseca, Redox properties of (1-(2-pyridylazo)-2-naphthol)copper(II) encapsulated in Y zeolite, Microporous Mesoporous Mater. 117 (2009) 297–303, https://doi.org/10.1016/j.micromeso.2008.07.005.
[33] E.R. Bandala, R. Sadek, J. Gurgul, K. Łątka, M. Zimowska, L. Valentin, O. M. Rodriguez-Narvaez, S. Dzwigaj, Assessment of the capability of Fe and Al modified BEA zeolites to promote advanced oxidation processes in aqueous phase, Chem. Eng. J. 409 (2021) 127379, https://doi.org/10.1016/j.cej.2020.127379.
[34] P. Yan, M.M.-J. Li, E. Kennedy, A. Adesina, G. Zhao, A. Setiawan, M. Stockenhuber, The role of acid and metal sites in hydrodeoxygenation of guaiacol over Ni/Beta catalysts, Catal. Sci. Technol. 10 (2020) 810, https://doi.org/10.1039/c9cy01970g.
[35] R. Kefirov, A. Penkova, K. Hadjiivanov, S. Dzwigaj, M. Che, Stabilization of Cu+ ions in BEA zeolite: study by FTIR spectroscopy of adsorbed CO and TPR, Microporous Mesoporous Mater. 116 (2008) 180–187, https://doi.org/10.1016/j.micromeso.2008.03.032.
[36] P. Sazama, E. Tabor, P. Klein, B. Wichterlova, S. Sklenak, L. Mokrzycki, V. Pashkkova, M. Ogura, J. Dedecek, Al-rich beta zeolites. Distribution of Al atoms in the framework and related protonic and metal-ion species, J. Catal. 333 (2016) 102–114, https://doi.org/10.1016/j.jcat.2015.10.010.
[37] C. Bisio, G. Martra, S. Coluccia, P. Massiani, FT-IR evidence of two distinct protonic sites in BEA zeolite: consequences on cationic exchange and on acid-basic properties in the presence of cesium, J. Phys. Chem. C 112 (2008) 10520–10530, https://doi.org/10.1021/jp7120017.
[38] M.L. Rache, A.R. García, H.R. Zea, A.M.T. Silva, L.M. Madeira, J.H. Ramírez, Azo-dye orange II degradation by the heterogeneous Fenton-like process using a zeolite Y-Fe catalyst—kinetics with a model based on the Fermi's equation, Appl. Catal., B 146 (2014) 192–200, https://doi.org/10.1016/j.apcatb.2013.04.028.
[39] B.L.C. Santos, P. Parpot, O.S.G.P. Soares, M.F.R. Pereira, E. Rombi, A.M. Fonseca, I. C. Neves, Fenton-type bimetallic catalysts for degradation of dyes in aqueous solutions, Catalysts 11 (2021) 32, https://doi.org/10.3390/catal11010032.